Retrieving the Size of Deep-Subwavelength Objects via Tunable Optical Spin-Orbit Coupling

Xi, Zheng; Urbach, H. P.

DOI
10.1103/PhysRevLett.120.253901

Publication date
2018

Document Version
Final published version

Published in
Physical Review Letters

Retrieving the Size of Deep-Subwavelength Objects via Tunable Optical Spin-Orbit Coupling

Zheng Xi* and H. P. Urbach
Optics Reseach Group, Delft University of Technology, Department of Imaging Physics, Lorentzweg 1, 2628CJ Delft, The Netherlands

(Received 1 February 2018; published 19 June 2018)

We propose a scheme to retrieve the size parameters of a nanoparticle on a glass substrate at a scale much smaller than the wavelength. This is achieved by illuminating the particle using two plane waves to create rich and nontrivial local polarization distributions, and observing the far-field scattering pattern into the substrate. By using this illumination to control the induced complex dipole moment, the exponential decay of power radiated into the supercritical region, as well as directional scattering due to spin-orbit coupling can be exploited to retrieve the particle's shape, size, and position directly from the far-field scattering with high sensitivity and without the need for a complicated and time-consuming optimization algorithm. Our method brings about a far-field superresolution nanometrology scheme based on the interaction of vectorial light with nanoparticles.

DOI: 10.1103/PhysRevLett.120.253901

The great interest in nanotechnology demands a simple, noninvasive, and far-field optical technique that is able to provide precise information about the shape and size of individual nanoparticles in order to monitor and use their size-dependent properties. The most straightforward way is to put the nanoparticle under an optical microscope. By exploiting the exponential decay of the evanescent field, subwavelength information of the height of the particle can be extracted [1–3]. However, the transverse dimension is limited by the diffraction limit. While the breakthrough in superresolution fluorescent microscopy makes use of nonlinear optical effects to achieve superresolution via isolation and localization of single fluorescent molecules [4–7], this approach cannot be applied directly to the case of nonfluorescent nanoparticles.

A light field that contains inhomogeneous polarization distributions has attracted great attention [8–13]. Of particular interest is the local transverse spin in optical fields [12,14,15]. In analogy to the spin-Hall effect of electrons, photons of different spins are found to couple to different directions. This intrinsic spin-dependent propagation not only initiated innovative studies in classical optics [16–22], but also is considered as a fundamental building block of future chiral quantum networks [23–26]. Most of the previous research focused on the forward problem: encoding the spin information into different directions of propagation [12,27–29]. In this Letter, we try to tackle the inverse problem: retrieving the subwavelength dimension of nanoparticles based on tunable spin-dependent scattering into the far field. In particular, we consider two cases of nanoparticles lying flat on a glass substrate with $n_{\mathrm{glass}} = 1.5$: a nanowire of subwavelength elliptical cross section characterized by two independent axes (2D case), and an ellipsoidal nanoparticle characterized by three independent axes (3D case). The material of the particle is chosen to be silicon with refractive index $n = 3.5$ to match the standard silicon-on-insulator technology. By illuminating the nanoparticle with an interference field and adjusting simple dipole scatttering models, the exponential decay of the scattered power beyond the critical angle can be used to retrieve the particle's height, while the local spin-driven directional scattering can be used to retrieve the transverse-to-vertical aspect ratio. This inversion scheme directly links the far-field scattering with deep-subwavelength information of the nanoparticle without sophisticated and time-consuming optimization algorithms, opening new possibilities for the future optical metrology methods exploiting the local interaction of vectorial light and matter.

To start with, we consider the 2D case of the emission of a general dipole $\vec{p} = [p_x, p_z]$ above a glass substrate with the surface normal parallel to the z axis. Since the scattering of a Rayleigh particle can be well described by this model, this serves as the theoretical foundation of the scheme.

The dipole is put in air with a distance z_0 from the interface. The magnetic field radiated into the substrate can be described by the angular spectrum method [30,31]:

$$H_y(k_x) = A_0 k_{zg} t_p \left(p_x + \frac{k_x}{k_{za}} p_z \right) e^{ik_{za} z_0}, \tag{1}$$

where $k_{zg} = \sqrt{n_g^2 k_0^2 - k_x^2}$, $k_{za} = \sqrt{k_0^2 - k_x^2}$ are the vertical wave vectors in glass and in air, k_0 is the wave number in air, n_g is the refractive index of glass, A_0 is a scaling factor, and t_p is the Fresnel coefficient. The term $e^{ik_{za} z_0}$ in Eq. (1)

separates propagating ($k_x \leq k_0$, k_{za} is real) and evanescent waves ($k_x > k_0$, k_{za} is imaginary) into two regions defined by the critical angle: the undercritical angle region (UAR) and supercritical angle region (SAR) [Fig. 1(a)]. We first consider a horizontal dipole, i.e., $p_z = 0$, and change the dipole-to-interface distance z_0 from $0.005\lambda_0$ to $0.1\lambda_0$. The power in the SAR comes from evanescent waves and thus increases exponentially as $e^{-|k_{za}|z_0}$ when z_0 decreases. In contrast, the power within the UAR originates from propagating waves. It only gains an extra phase term $e^{ik_{za}z_0}$ leaving the total power in this region unchanged. The power ratio of the scattered field in the UAR and the SAR can be calculated as a function of z_0 and the result is shown in Fig. 1(b). The exponential decay of the power ratio can be used to extract the vertical position of the dipole, even at deep subwavelength scale as was shown in Refs. [1–3]. Next we consider a more general case: a spin dipole with $p_z = i\gamma p_x$ with varying γ from 0 to 1 [Figs. 1(c) and 1(d)]. The additional spin introduced $\pi/2$ phase difference breaks the symmetry depending on the handedness of the dipole [12]. This in turn leads to the uneven distribution of the angular spectrum for $k_x > k_0$, which can then be translated into asymmetric propagation in the SAR [Fig. 1(c)]. This spin-dependent directional emission is very sensitive to the value of γ. In Fig. 1(d), we plot the integrated power ratio into the right supercritical angle region (RSAR) and left supercritical angle region (LSAR) against different γ at $z_0 = 0.005\lambda_0$. An optimum $\gamma_{\text{opt}} = 0.5$ that yields the largest asymmetry is clearly visible.

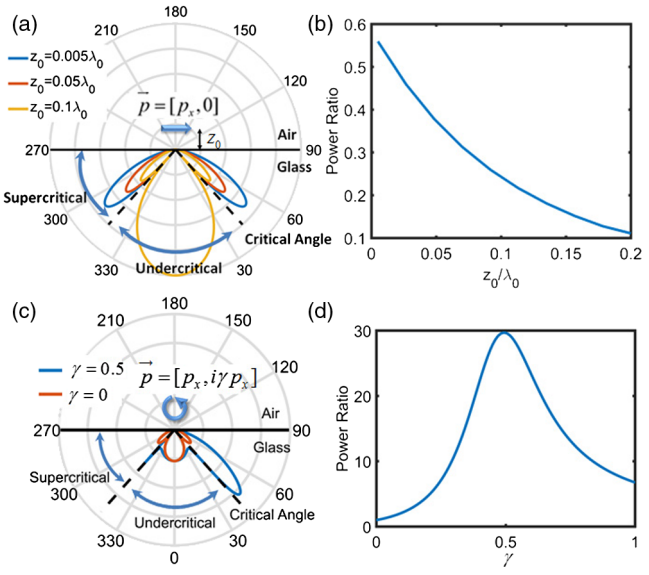

FIG. 1. (a) Far-field radiation pattern into the glass substrate when a horizontal dipole p_x is placed at different distances z_0 from the interface. The radiation pattern in UAR is the same for all z_0. (b) Power ratio between the SAR and the UAR as the horizontal dipole is moved away from the interface. (c) Far-field radiation pattern into the glass substrate for a spin dipole. (d) Power ratio between the RSAR and the LSAR for different γ for a general spin dipole located at $z_0 = 0.005\lambda_0$.

From the above discussions, we have seen for a simple dipole model that the far field changes significantly with the proper choice of the complex dipole moment. Precise information about the dipole's vertical position z_0 as well as the optimum ratio γ_{opt} between different dipole moments can be extracted from far-field measurements. Replacing the dipole by a Rayleigh particle, we wonder if it is possible to develop a quantitative approach to retrieve subwavelength information about the particle based on the same principle.

We first consider the 2D case: a silicon nanowire with an elliptical cross section characterized by two axes of lengths a and b in the x and z directions, respectively. The nanowire is sitting on a glass substrate. This geometry is widely used in nano-waveguide applications. The cross-section profile plays an important role in the determination of the overall performance of the waveguide. The aim here is to retrieve the length of the two axes a and b from the far-field measurements. For this purpose, the illumination field is designed to be two p-polarized plane waves forming an interference pattern along the air-glass interface shown in Fig. 2(a). To simplify the discussion, the incident angle is chosen to be at the Brewster angle θ_p for both beams. The illumination field above the interface can be calculated analytically [31]:

$$E_x = 2E_0 \cos\theta_p \cos(k_x x),$$
$$E_z = 2iE_0 \sin\theta_p \sin(k_x x), \tag{2}$$

where E_0 is the amplitude of the incident beam and k_x is the transverse wave vector component in air. Interestingly, even for this seemingly simple field, it contains rich local polarization topology distributions along the x axis [21]. Starting from $x = 0$ as indicated by the dashed line in Fig. 2(a), the local polarization state changes from linear to circular polarizations of different handedness on each side. This polarization change is within the subwavelength scale. If a detection scheme can be developed such that it responds only to a certain polarization state, the slight deviation from that polarization state would cause significant changes in observables, making the scheme very sensitive [16,22].

To utilize this, we consider a nanowire of a certain shape parameters a and b placed inside the field and calculate the power ratio in RSAR and LSAR at different x for different shapes [Fig. 2(b)]. When the local polarization state at a certain displacement x_0 matches the shape of the cross section, resulting in optimum γ_{opt} between induced complex dipole moments, the power in the SAR becomes highly asymmetric [peaks in Fig. 2(b)]. As a result, different shape information is encoded in the displacement measurement along x.

To decode the relation between the displacement and the shape parameters, an analytical model can be derived.

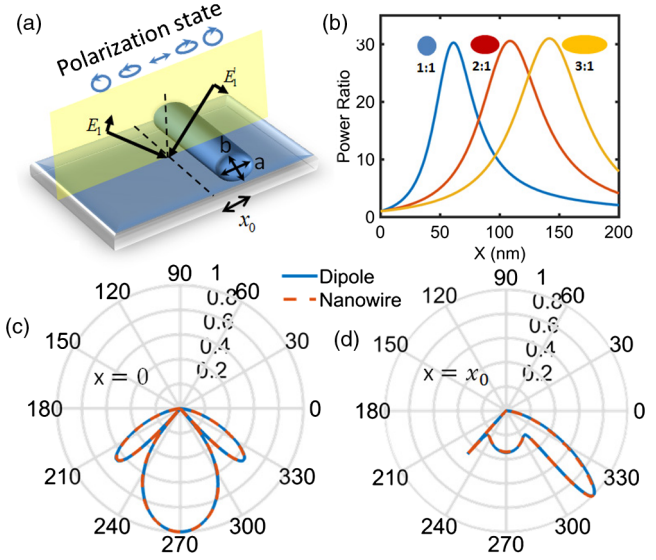

FIG. 2. (a) Geometry of the considered 2D system. A nanowire is placed on top of a glass substrate. Two p-polarized plane waves are incident at the Brewster angle on the nanowire, forming an interference pattern. The nanowire is moved along the x axis. The polarization state along x changes from linear to circular of different handedness as schematically shown by the blue arrows and circles. (b) Power ratio in the RSAF and LSAF region as the nanowire is moving along x. The insets show different shapes of the cross sections with aspect ratio $a:b = 1:1$(blue), $2:1$(red), and $3:1$(yellow) when $b = 10$ nm. (c) Far-field scattering (red dashed curve) pattern of a nanowire placed at $x = 0$ into the substrate simulated by COMSOL. The scattering pattern can be well described by an equivalent horizontal dipole placed at the center of the nanowire (blue curve). (d) Same as Fig. 2(c) except the nanowire is placed at $x = x_0$ and can be approximated by a spin dipole with γ_{opt}.

Within the Born approximation (i.e., surface dressing of the polarizability is neglected) and assuming a, $b \ll \lambda$, the two components of the induced dipole inside the nanowire can be written as

$$p_x = \alpha_x E_x, \qquad p_z = \alpha_z E_z, \tag{3}$$

with the polarizability related to the geometry parameters [32]

$$\alpha_i = V \frac{\epsilon_r - 1}{1 + L_i(\epsilon_r - 1)} \qquad i = x, z, \tag{4}$$

where ϵ_r is the relative permittivity of the nanowire, $L_x = [a/(a+b)]$, $L_z = [b/(a+b)]$ corresponds to the geometry of the cross section and $V = \pi^2 ab$.

Combining Eqs. (3) and (4), the ratio between the induced dipole components can be calculated as

$$\frac{p_x}{p_z} = \frac{s + \epsilon_r}{1 + s\epsilon_r} \frac{E_x}{E_z}, \tag{5}$$

with $s = a/b$ the aspect ratio of the two axes, which relates the geometry of the two axes with the induced dipoles.

When the background field is taken to be as in Eq. (2), the above expression can be written as

$$\frac{p_x}{p_z} = i \cot\theta_p \cot(k_x x) \frac{s + \epsilon_r}{1 + s\epsilon_r}; \tag{6}$$

hence, a general dipole with a changing ellipticity depending on the location x is induced. Consider the range $x \in \{-[\pi/(2k_x)], [\pi/(2k_x)]\}$. Only at $x = 0$, the illumination field is linearly x polarized, and the nanowire can be approximated by a linearly x-polarized dipole situated at the center of the nanowire [Fig. 2(c)]. The scattered field into the substrate in this case is symmetric. The vertical position of the induced dipole corresponds to the height $b/2$ of the nanowire, and can be extracted from the power ratio between UAR and SAR. Because the local polarization state changes continuously along x, at a certain displacement x_0 from the origin, the nanowire becomes a spin dipole with optimized γ_{opt} [Fig. 2(d)]. By substituting γ_{opt} into Eq. (6) one can get the solution for the aspect ratio s:

$$s = \frac{\epsilon_r - A}{A\epsilon_r - 1}, \tag{7}$$

where $A = \tan(\theta_p)\tan(k_x x_0)/|\gamma_{\mathrm{opt}}|$. This simple expression relates the aspect ratio s directly to the optimum displacement x_0, which yields the largest asymmetry in the far field. From the aspect ratio s and the length of the vertical axis b, the transverse dimension a can be retrieved. This far-field measurement approach gives information of the particles shape (aspect ratio s), size (length of the two axes a and b), and location x_0 at the same time.

In Fig. 3, several geometries with different parameters are tested. We use commercial software COMSOL to simulate the forward far-field scattering problem and retrieve the parameters using the simulated data. The illumination wavelength is chosen to be 1000 nm for all cases. Figure 3(a) shows the retrieval of the height of a

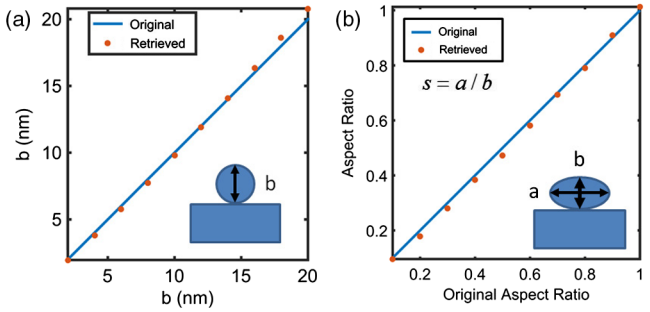

FIG. 3. (a) Retrieval of the height b of silicon nanowires of a circular cross section from the power ratio in the UAR and SAR. (b) Retrieval of the aspect ratio from the power ratio of the RSAR and LSAR. The height b is fixed as 10 nm.

silicon nanowire with a circular cross section. The only unknown here is the length of the vertical axis b. For the retrieval of the aspect ratio s, b is fixed at 10 nm. The results are shown in Fig. 3(b). In both cases, the retrieved results match the original design quite well.

The above discussions are for 2D nanowaveguide applications, the proposed scheme can be applied to a general 3D case as well. The 3D particle can be described by an ellipsoidal nanorod with three axes a, b, and c shown in Fig. 4(a). We assume the orientation of the nanorod can be determined by simple in-plane polarization analysis [33]. The main goal here is to retrieve a, b, and c.

The vertical dimension c can be retrieved as before by looking at the power ratio in SAR and UAR. For a and b, two successive illuminations are applied with p-polarized plane waves along the YZ and XZ planes, respectively. The induced dipoles at the optimum displacement x_0 and y_0 can be calculated as

$$\frac{p_x}{p_z} = i\frac{\alpha_x}{\alpha_z}\cot\theta_p \cot k_x x_0 = \frac{1}{i|\gamma_{\text{opt}}|},$$
$$\frac{p_y}{p_z} = i\frac{\alpha_y}{\alpha_z}\cot\theta_p \cot k_y y_0 = \frac{1}{i|\gamma_{\text{opt}}|}, \tag{8}$$

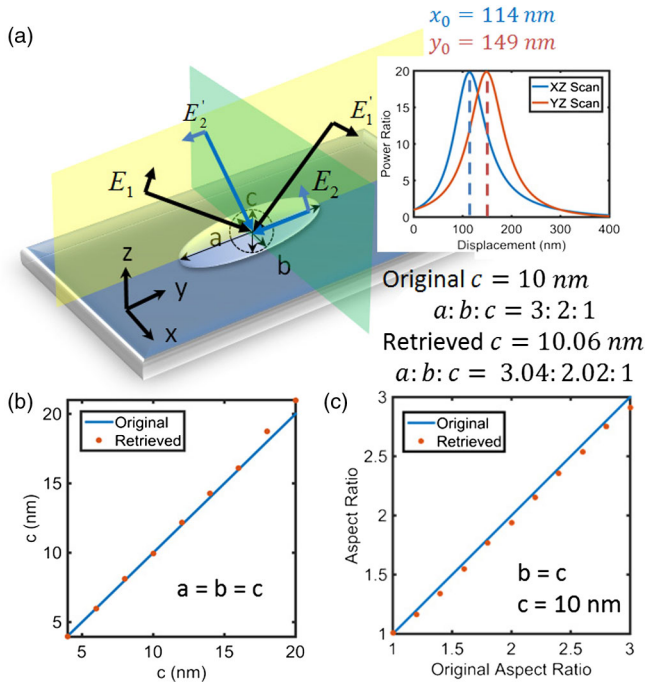

FIG. 4. (a) Geometry of the considered 3D system. A nanorod is placed on a glass substrate. Two successive illuminations in the YZ (yellow) plane and XZ (green) plane are used to illuminate the nanorod. The calculated optimum displacements x_0 and y_0 are shown in the top-right inset for a nanorod of dimensions $a = 30$, $b = 20$, and $c = 10$ nm. Bottom right is the retrieved parameters. (b) Retrieval of the radius of a nanosphere. (c) Retrieval of the aspect ratio a/c of different nanorods with fixed height $c = 10$ nm.

with α_x, α_y, and α_z determined analogously to Eq. (4) [32]. By substituting Eq. (4) into Eq. (8), we get

$$A(\epsilon_r - 1)L_1 - (\epsilon_r - 1)L_3 = 1 - A,$$
$$B(\epsilon_r - 1)L_2 - (\epsilon_r - 1)L_3 = 1 - B, \tag{9}$$

in which ϵ_r is the permittivity of the nanorod, $A = \tan\theta_p \tan(k_y y_0)/|\gamma_{\text{opt}}|$ and $B = \tan\theta_p \tan(k_x x_0)/|\gamma_{\text{opt}}|$. Equation (8) together with the requirement that [32]

$$L_1 + L_2 + L_3 = 1 \tag{10}$$

can be used to solve L_1, L_2, and L_3 based on the measured values of x_0 and y_0. To further relate these values to the geometrical parameters a, b, and c, we compare the L_1, L_2, and L_3 with the theoretically calculated ones according to [32]

$$L_i = \int_0^\infty \frac{l_i l_j l_k dm}{2(m + l_i^2)^{3/2}(m + l_j^2)^{1/2}(m + l_k^2)^{1/2}}, \tag{11}$$

in which $l_{i,j,k} = a/2$, $b/2$, and $c/2$, respectively, by varying a, b, and c to get the best match.

As one example, we consider a silicon nanorod sitting on a glass substrate. The illumination wavelength is chosen at 1000 nm. The three axes of the nanorod are chosen as $a = 30$, $b = 20$, and $c = 10$ nm. The calculated power ratios in the SAR are plotted in the inset of Fig. 4(a). From the peaks of these curves, the optimum displacements $x_0 = 114$ and $y_0 = 149$ nm can be extracted. Substituting these values into Eqs. (9)–(11), the information of the three axes are retrieved and the results are listed at the bottom right of Fig. 4(a).

For most situations, the nanorod can be approximated by a prolate spheroid ($a > b = c$). We have also investigated this case and the results are shown in Figs. 4(b) and 4(c). The retrieval of the length of the vertical axis c is shown in Fig. 4(b). Nanospheres of changing radius c are considered as examples for retrieval. In Fig. 4(c), the vertical axis is fixed at $c = 10$ nm and the different aspect ratios a/c are retrieved.

Finally, it is also worth mentioning that the displacement of the particle can be equivalently treated as changing the phase of one of the incident plane waves. Because the control over phase can be very accurate, this method may be beneficial from an experimental point of view.

In conclusion, we have proposed a method to retrieve information about the shape, size, and location of a particle at a deep subwavelength scale. We note that the upper limit of the particle's size is imposed by the condition that the wavelength inside the particle is much smaller than the particle's size so that the quasistatic approximation for the polarizability holds (i.e., nk_0a, $nk_0b \ll 1$ for the 2D case, where n is the refractive index of the particle and k_0

the free-space wave number). However, the method can be extended to larger particles by correcting the reference model based on COMSOL simulations as explained in the Supplemental Material [31]. The hard problem of extracting subwavelength information is converted into the measurement of the symmetry of the scattering pattern at different locations. The method utilizes the full vectorial interaction of light and particle, in particular, the photonic spin-orbit interaction, and it also serves as a guideline for the development of ultrasensitive displacement sensors by shaping nanoparticles [13,22,34,35]. Additionally, because the model retrieves the complex dipole vector properties, it may also find interesting applications to image complex dipole vectors of a single molecule [36–39]. This spin-based retrieval method can have important applications in ultrahigh resolution nanometrology and can shed new light on superresolution techniques involving the interaction of vectorial light and matter.

The authors would like to thank Sander Konijnenberg for stimulating discussions on the implementations of different noise models.

*z.xi@tudelft.nl

[1] N. Bourg, C. Mayet, G. Dupuis, T. Barroca, P. Bon, S. Lcart, E. Fort, and S. Lvque-Fort, Nat. Photonics **9**, 587 (2015).

[2] T. Barroca, K. Balaa, S. Lévêque-Fort, and E. Fort, Phys. Rev. Lett. **108**, 218101 (2012).

[3] C. M. Winterflood, T. Ruckstuhl, D. Verdes, and S. Seeger, Phys. Rev. Lett. **105**, 108103 (2010).

[4] S. W. Hell and J. Wichmann, Opt. Lett. **19**, 780 (1994).

[5] E. Betzig, J. Trautman, T. Harris, J. Weiner, and R. Kostelak, Science **251**, 1468 (1991).

[6] B. Huang, W. Wang, M. Bates, and X. Zhuang, Science **319**, 810 (2008).

[7] S. Bretschneider, C. Eggeling, and S. W. Hell, Phys. Rev. Lett. **98**, 218103 (2007).

[8] A. F. Abouraddy and K. C. Toussaint, Phys. Rev. Lett. **96**, 153901 (2006).

[9] R. Dorn, S. Quabis, and G. Leuchs, Phys. Rev. Lett. **91**, 233901 (2003).

[10] A. B. Young, A. C. T. Thijssen, D. M. Beggs, P. Androvitsaneas, L. Kuipers, J. G. Rarity, S. Hughes, and R. Oulton, Phys. Rev. Lett. **115**, 153901 (2015).

[11] T. Zhang, Y. Ruan, G. Maire, D. Sentenac, A. Talneau, K. Belkebir, P. C. Chaumet, and A. Sentenac, Phys. Rev. Lett. **111**, 243904 (2013).

[12] F. J. Rodrguez-Fortuo, G. Marino, P. Ginzburg, D. OConnor, A. Martnez, G. A. Wurtz, and A. V. Zayats, Science **340**, 328 (2013).

[13] Z. Xi, L. Wei, A. J. L. Adam, H. P. Urbach, and L. Du, Phys. Rev. Lett. **117**, 113903 (2016).

[14] A. Aiello, P. Banzer, M. Neugebauer, and G. Leuchs, Nat. Photonics **9**, 789 (2015).

[15] K. Y. Bliokh, F. Rodríguez-Fortuño, F. Nori, and A. V. Zayats, Nat. Photonics **9**, 796 (2015).

[16] M. Neugebauer, T. Bauer, P. Banzer, and G. Leuchs, Nano Lett. **14**, 2546 (2014).

[17] D. O'connor, P. Ginzburg, F. Rodríguez-Fortuño, G. Wurtz, and A. Zayats, Nat. Commun. **5**, 5327 (2014).

[18] F. J. Rodríguez-Fortuño, N. Engheta, A. Martínez, and A. V. Zayats, Nat. Commun. **6**, 8799 (2015).

[19] M. Antognozzi, C. R. Bermingham, R. L. Harniman, S. Simpson, J. Senior, R. Hayward, H. Hoerber, M. R. Dennis, A. Y. Bekshaev, K. Y. Bliokh, and F. Nori, Nat. Phys. **12**, 731 (2016).

[20] M. Neugebauer, T. Bauer, A. Aiello, and P. Banzer, Phys. Rev. Lett. **114**, 063901 (2015).

[21] A. Y. Bekshaev, K. Y. Bliokh, and F. Nori, Phys. Rev. X **5**, 011039 (2015).

[22] O. G. Rodriguez-Herrera, D. Lara, K. Y. Bliokh, E. A. Ostrovskaya, and C. Dainty, Phys. Rev. Lett. **104**, 253601 (2010).

[23] P. Lodahl, S. Mahmoodian, S. Stobbe, A. Rauschenbeutel, P. Schneeweiss, J. Volz, H. Pichler, and P. Zoller, Nature (London) **541**, 473 (2017).

[24] R. Coles, D. Price, J. Dixon, B. Royall, E. Clarke, P. Kok, M. Skolnick, A. Fox, and M. Makhonin, Nat. Commun. **7**, 11183 (2016).

[25] R. Mitsch, C. Sayrin, B. Albrecht, P. Schneeweiss, and A. Rauschenbeutel, Nat. Commun. **5** (2014).

[26] C. Sayrin, C. Junge, R. Mitsch, B. Albrecht, D. OShea, P. Schneeweiss, J. Volz, and A. Rauschenbeutel, Phys. Rev. X **5**, 041036 (2015).

[27] B. Le Feber, N. Rotenberg, and L. Kuipers, Nat. Commun. **6**, 6695 (2015).

[28] I. Sllner, S. Mahmoodian, S. L. Hansen, L. Midolo, A. Javadi, G. Kiransk, T. Pregnolato, H. El-Ella, E. H. Lee, J. D. Song, S. Stobbe, and P. Lodahl, Nat. Nanotechnol. **10**, 775 (2015).

[29] J. Petersen, J. Volz, and A. Rauschenbeutel, Science **346**, 67 (2014).

[30] L. Novotny and B. Hecht, *Principles of Nano-Optics* (Cambridge University Press, Cambridge, England, 2012).

[31] See Supplemental Material at http://link.aps.org/supplemental/10.1103/PhysRevLett.120.253901 for a detailed derivation of Eqs. (1) and (2), discussions on the differences between linear dipole and spin dipole, retrieval of the aspect ratio using noisy data and retrieval procedure for larger aspect ratios.

[32] H. C. Hulst and H. C. van de Hulst, *Light Scattering by Small Particles* (Courier Corporation, New York, 1957).

[33] T. Li, Q. Li, Y. Xu, X.-J. Chen, Q.-F. Dai, H. Liu, S. Lan, S. Tie, and L.-J. Wu, ACS Nano **6**, 1268 (2012).

[34] M. Neugebauer, P. Woniak, A. Bag, G. Leuchs, and P. Banzer, Nat. Commun. **7**, 11286 (2016).

[35] Z. Xi and H. P. Urbach, Phys. Rev. Lett. **119**, 053902 (2017).

[36] L. Novotny, M. R. Beversluis, K. S. Youngworth, and T. G. Brown, Phys. Rev. Lett. **86**, 5251 (2001).

[37] C. Lethiec, J. Laverdant, H. Vallon, C. Javaux, B. Dubertret, J.-M. Frigerio, C. Schwob, L. Coolen, and A. Maitre, Phys. Rev. X **4**, 021037 (2014).

[38] B. Sick, B. Hecht, and L. Novotny, Phys. Rev. Lett. **85**, 4482 (2000).

[39] M. R. Foreman, C. M. Romero, and P. Török, Opt. Lett. **33**, 1020 (2008).